

# The dual reciprocity boundary element formulation for convection-diffusion-reaction problems with variable velocity field using different radial basis functions

Salam Adel AL-Bayati<sup>a,\*</sup>, Luiz C. Wrobel<sup>a,b</sup>

<sup>a</sup>College of Engineering, Design and Physical Sciences, Brunel University London, Uxbridge, UB8 3PH, UK

<sup>b</sup>Institute of Materials and Manufacturing, Brunel University London, Uxbridge, UB8 3PH, UK

---

## Abstract

This paper presents a dual reciprocity boundary element method (DRBEM) formulation for the solution of steady-state convection-diffusion-reaction problems with variable velocity field at moderately high Péclet number. This scheme is based on utilising the fundamental solution of the convection-diffusion-reaction equation with constant coefficients. In this case, we decompose the velocity field into an average and a perturbation, with the latter being treated using a dual reciprocity approximation to convert the domain integrals arising in the boundary element formulation into equivalent boundary integrals. A proposed approach is implemented to treat the convective terms with variable velocity, for which the concentration is expanded as a series of functions. Four numerical experiments are included with available analytical solutions, to establish the validity of the approach and to demonstrate the efficiency of the proposed method.

*Keywords:* BEM, dual reciprocity technique, convection-diffusion-reaction, variable velocity field, radial basis function

---

## 1. Introduction

The boundary element method (BEM) has been applied to steady-state convection-diffusion-reaction problems with variable velocity by various researchers [1, 2, 3, 4, 5, 6, 7, 8, 9]. However, the solution of this problem is still considered a big challenge, particularly for variable and high velocities. The BEM does  
5 have an inherent advantage for the solution of convection-diffusion-reaction problems with constant velocity as the existing fundamental solution of the problem introduces the exact amount of upwind, contrary to finite element or finite-difference methods where the upwind is numerical [7]. The dual reciprocity boundary element method (DRBEM) represents an alternative for solving linear PDEs with variable coefficients [10, 11, 12, 13, 14]. The solution of problems involving variable coefficients is more difficult to achieve with the  
10 BEM as fundamental solutions are only available for a small number of cases, for coefficients with very simple variations in space. The approach adopted in this paper is to split the velocity field into an average and a perturbation; the average velocity (constant) is included in the fundamental solution, while the perturbation

---

\*Corresponding author,

*Email addresses:* Salam.AL-Bayati@brunel.ac.uk (Salam Adel AL-Bayati), Luiz.Wrobel@brunel.ac.uk (Luiz C. Wrobel)

generates a domain integral which is treated with the DRBEM. A new particular solution has been used with corresponding dual reciprocity expressions. A proposed approach was implemented to treat the convective terms with variable velocity. Results of four test cases are presented and compared to analytical solutions. They show that the boundary element formulation developed in this work produces accurate results for diffusion-dominated problems with low velocity values.

A brief outline of the rest of this paper is as follows. Section 2 reviews the representation of convection-diffusion-reaction problems. Section 3 derives the boundary element formulation using the steady-state fundamental solution of the corresponding equation. In section 4, the DRM formulation is developed for 2D steady-state convection-diffusion-reaction problem, followed in section 5 by a description of the discretisation of the DRBEM formulation for this model. Handling the convective terms by expanding the relevant functions as a series are shown in section 6. Section 7 gives the description of the coordinate functions and the three radial basis functions adopted in this work. Section 8 compares and discusses the solution profiles for the present numerical experiments. Computational aspects are included to demonstrate the performance of this approach in section 9. Finally, some conclusions are provided in the last section.

## 2. Convection-diffusion-reaction equation

The two-dimensional convection-diffusion-reaction problem over a domain  $\Omega$  in  $\mathbb{R}^2$  limited by a boundary  $\Gamma$ , for isotropic materials, is governed by the following PDE:

$$D\nabla^2\phi(x, y) - v_x(x, y)\frac{\partial\phi(x, y)}{\partial x} - v_y(x, y)\frac{\partial\phi(x, y)}{\partial y} - k\phi(x, y) = 0 \quad (1)$$

$$x, y \in \Omega \subset \mathbb{R}^d, t > 0$$

In Eq.(1),  $\phi$  represents the concentration of a substance, treated as a function of space,  $\Gamma$  is a bounded domain in  $\mathbb{R}^d$ ,  $d$  is the dimension of the problem. The velocity components  $v_x$  and  $v_y$  along the x and y directions and assumed to vary in space. Besides,  $D$  is the diffusivity coefficient and  $k$  represents the first-order reaction constant or adsorption coefficient. The boundary conditions are

$$\phi = \bar{\phi} \quad \text{over} \quad \Gamma_D \quad (2)$$

$$q = \frac{\partial\phi}{\partial n} = \bar{q} \quad \text{over} \quad \Gamma_N \quad (3)$$

where  $\Gamma_D$  and  $\Gamma_N$  are the Dirichlet and Neumann parts of the boundary with  $\Gamma = \Gamma_D \cup \Gamma_N$ .

The parameter that describes the relative influence of the convective and diffusive components is called Péclet number,  $Pé = |v|L/D$ , where  $v$  is the velocity field and  $L$  is the characteristic length of the domain. For small values of  $Pé$ , Eq.(1) behaves as a parabolic differential equation, while for large values of  $Pé$  the equation becomes more like hyperbolic. These changes in the structure of the differential equation according to the values of the Péclet number have significant effects on its numerical solution.

### 3. Boundary element formulation of convection-diffusion-reaction problems using steady-state fundamental solution

35

For the sake of obtaining an integral equation equivalent to the above partial differential equation, a fundamental solution of Eq.(1) is necessary. However, fundamental solutions are only available for the case of constant velocity fields. Thus, the variable velocity components  $v_x = v_x(x, y)$  and  $v_y = v_y(x, y)$  are decomposed into average (constant) terms  $\bar{v}_x$  and  $\bar{v}_y$ , and perturbations  $P_x = P_x(x, y)$  and  $P_y = P_y(x, y)$ , such that

40

$$\begin{aligned} v_x(x, y) &= \bar{v}_x + P_x(x, y) \\ v_y(x, y) &= \bar{v}_y + P_y(x, y) \end{aligned} \quad (4)$$

This permits rewriting equation (1) as

$$D\nabla^2\phi - \bar{v}_x\frac{\partial\phi}{\partial x} - \bar{v}_y\frac{\partial\phi}{\partial y} - k\phi = P_x\frac{\partial\phi}{\partial x} + P_y\frac{\partial\phi}{\partial y} \quad (5)$$

The above differential equation can now be transformed into the following equivalent integral equation

$$\phi(\xi) - D\int_{\Gamma}\phi^*\frac{\partial\phi}{\partial n}d\Gamma + D\int_{\Gamma}\phi\frac{\partial\phi^*}{\partial n}d\Gamma + \int_{\Gamma}\phi\phi^*\bar{v}_n d\Gamma = -\int_{\Omega}\left(P_x\frac{\partial\phi}{\partial x} + P_y\frac{\partial\phi}{\partial y}\right)\phi^*d\Omega \quad (6)$$

where  $\bar{v}_n = \bar{v}\cdot n$ ,  $n$  is the unit outward normal vector and the dot stands for scalar product. In the above equation,  $\phi^*$  is the fundamental solution of the convection-diffusion-reaction equation with constant coefficients. For two-dimensional problems,  $\phi^*$  is of the form

$$\phi^*(\xi, \chi) = \frac{1}{2\pi D} e^{-\left(\frac{\bar{v}\cdot r}{2D}\right)} K_0(\mu r) \quad (7)$$

where

$$\mu = \left[\left(\frac{\bar{v}}{2D}\right)^2 + \frac{k}{D}\right]^{\frac{1}{2}} \quad (8)$$

in which  $\xi$  and  $\chi$  are the source and field points, respectively, and  $r$  is the modulus of  $\mathbf{r}$ , the distance vector between the source and field points. The derivative of the fundamental solution with respect to the outward normal direction is given by

$$\frac{\partial\phi^*}{\partial n} = \frac{1}{2\pi D} e^{-\left(\frac{\bar{v}\cdot r}{2D}\right)} \left[-\mu K_1(\mu r) \frac{\partial r}{\partial n} - \frac{\bar{v}_n}{2D} K_0(\mu r)\right] \quad (9)$$

In the above,  $K_0$  and  $K_1$  are Bessel functions of second kind, of orders zero and one, respectively (for more details of the fundamental solution and its normal derivative, see [4, 6, 10]). The exponential term is responsible for the inclusion of the correct amount of upwind into the formulation [7]. Eq.(6) is valid for source points  $\xi$  inside the domain  $\Omega$ . A similar expression can be obtained, by a limit analysis, for source points  $\xi$  on the boundary  $\Gamma$ , in the form

$$c(\xi)\phi(\xi) - D\int_{\Gamma}\phi^*\frac{\partial\phi}{\partial n}d\Gamma + D\int_{\Gamma}\phi\frac{\partial\phi^*}{\partial n}d\Gamma + \int_{\Gamma}\phi\phi^*\bar{v}_n d\Gamma = -\int_{\Omega}\left(P_x\frac{\partial\phi}{\partial x} + P_y\frac{\partial\phi}{\partial y}\right)\phi^*d\Omega \quad (10)$$

in which  $c(\xi)$  is a function of the internal angle the boundary  $\Gamma$  makes at point  $\xi$ .

#### 4. DRM formulation for steady-state convection-diffusion-reaction problem

In the present formulation, we concentrate on the implementation of the dual reciprocity formulation DRM based on the fundamental solution to the steady-state convection-diffusion-reaction equation, where the convective velocity is assumed to be variable and is split into two parts, constant and perturbation, respectively. The basic idea is to expand the non-homogenous perturbation term on the right-hand side of Eq.(5) in the form

$$P_x \frac{\partial \phi}{\partial x} + P_y \frac{\partial \phi}{\partial y} = \sum_{k=1}^M f_k \alpha_k \quad (11)$$

This series contains a sequence of known functions  $f_k = f_k(x, y)$ , and a set of unknown coefficients  $\alpha_k$ . Using this approximation, the domain integral in Eq.(10) can be approximated in the form

$$\int_{\Omega} \left( P_x \frac{\partial \phi}{\partial x} + P_y \frac{\partial \phi}{\partial y} \right) \phi^* d\Omega = \sum_{k=1}^M \alpha_k \int_{\Omega} f_k \phi^* d\Omega \quad (12)$$

The next step is to consider that, for each function  $f_k$ , there exists a related function  $\psi_k$  which is a particular solution of the equation

$$D\nabla^2 \psi - \bar{v}_x \frac{\partial \psi}{\partial x} - \bar{v}_y \frac{\partial \psi}{\partial y} - k\psi = f \quad (13)$$

Thus, the domain integral can be recast in the form

$$\int_{\Omega} \left( P_x \frac{\partial \phi}{\partial x} + P_y \frac{\partial \phi}{\partial y} \right) \phi^* d\Omega = \sum_{k=1}^M \alpha_k \int_{\Omega} \left( D\nabla^2 \psi_k - \bar{v}_x \frac{\partial \psi_k}{\partial x} - \bar{v}_y \frac{\partial \psi_k}{\partial y} - k\psi_k \right) \phi^* d\Omega \quad (14)$$

Substituting Eq.(14) into (10), and utilising integration by parts in the domain integral of the resulting equation, we finally obtain a boundary integral equation of the form

$$\begin{aligned} c(\xi) \phi(\xi) - D \int_{\Gamma} \phi^* \frac{\partial \phi}{\partial n} d\Gamma + D \int_{\Gamma} \phi \frac{\partial \phi^*}{\partial n} d\Gamma + \int_{\Gamma} \phi \phi^* \bar{v}_n d\Gamma \\ = \sum_{k=1}^M \alpha_k \left[ c(\xi) \psi_k(\xi) - D \int_{\Gamma} \phi^* \frac{\partial \psi_k}{\partial n} d\Gamma + D \int_{\Gamma} \psi_k \frac{\partial \phi^*}{\partial n} d\Gamma + \int_{\Gamma} \psi_k \phi^* \bar{v}_n d\Gamma \right] \end{aligned} \quad (15)$$

#### 45 5. Space discretisation of the 2D convection-diffusion-reaction model

For the sake of simplicity in the presentation, this section will demonstrate the discretisation of the problem. To discretise the spatial domain, boundary element formulations were employed. Eq.(15) can now be re-written in discretised form in which the integrals over the boundary are approximated by a summation of integrals over individual boundary elements, i.e.

$$c_i \phi_i - \sum_{j=1}^N D \int_{\Gamma_j} \phi^* \frac{\partial \phi}{\partial n} d\Gamma + D \sum_{j=1}^N \int_{\Gamma_j} \left( \frac{\partial \phi^*}{\partial n} + \frac{\bar{v}_n}{D} \phi^* \right) \phi d\Gamma \quad (16)$$

$$= \sum_{k=1}^M \alpha_k \left[ c_i \psi_{ik}(\xi) - D \sum_{j=1}^N \int_{\Gamma_j} \phi^* \frac{\partial \psi_k}{\partial n} d\Gamma + D \sum_{j=1}^N \int_{\Gamma_j} \left( \frac{\partial \phi^*}{\partial n} + \frac{\bar{v}_n}{D} \phi^* \right) \psi_k d\Gamma \right]$$

where the index  $i$  means the values at the source point  $\xi$  and  $N$  elements have been employed. The functions  $\phi, q = \partial\phi/\partial n, \psi$  and  $\eta = \partial\psi/\partial n$  within each boundary element are approximated in this study using constant elements. It should be remarked that functions  $\psi$  and  $\eta$  need not be approximated as they are known functions for a specified set  $f$ . However, doing so will greatly improve the computer efficiency of the technique with only a minor sacrifice in accuracy. Applying Eq.(16) to all boundary nodes using a collocation technique results in the following system of equations

$$H\phi - Gq = (H\psi - G\eta)\alpha \quad (17)$$

As shown in the above system, the same matrices  $H$  and  $G$  are used on both sides. Both  $\psi$  and  $\eta$  are geometry-dependent square matrices (assuming, for simplicity, that the number of terms in expression (12) is equal to the number of boundary nodes), and  $\phi, q$  and  $\alpha$  are vectors of nodal values. The next step in the formulation is to find an expression for the unknown vector  $\alpha$ . Applying Eq.(16) to all  $M$  nodes, it is possible to write the resulting set of equations in the following matrix form,

$$P_x \frac{\partial \phi}{\partial x} + P_y \frac{\partial \phi}{\partial y} = F\alpha \quad (18)$$

where  $P_x$  and  $P_y$  can be understood as two diagonal matrices with components  $P_x(x_i, y_i)$  and  $P_y(x_i, y_i)$ , respectively, while  $\frac{\partial \phi}{\partial x}$  and  $\frac{\partial \phi}{\partial y}$  are column vectors. Inverting expression (18), one arrives at

$$\alpha = F^{-1} \left( P_x \frac{\partial \phi}{\partial x} + P_y \frac{\partial \phi}{\partial y} \right) \quad (19)$$

Substituting into Eq.(17),

$$H\phi - Gq = (H\psi - G\eta) F^{-1} \left( P_x \frac{\partial \phi}{\partial x} + P_y \frac{\partial \phi}{\partial y} \right) \quad (20)$$

Defining a matrix  $S$  in the form

$$S = (H\psi - G\eta) F^{-1} \quad (21)$$

one can write Eq.(20) as

$$H\phi - Gq = S \left( P_x \frac{\partial \phi}{\partial x} + P_y \frac{\partial \phi}{\partial y} \right) \quad (22)$$

Once functions  $f_k$  are defined, matrix  $S$  can be established as this matrix depends on geometry only. Furthermore, the coefficients of matrices  $P_x$  and  $P_y$  are also known. Therefore, there remains to be found an expression relating the derivatives of  $\phi$  to reduce Eq.(22) to a standard BEM form.

50 **6. Handling convective terms**

In this section, emphasis will be placed on convective terms. A mechanism must be established to relate the nodal values of  $\phi$  to the nodal values of its derivatives. The function-expansion approach [15] has been implemented in this part of the work.

Assume that the function  $\phi$  can be represented by

$$\phi = \sum_{k=1}^M \mathfrak{S}_k \beta_k \quad (23)$$

We now start by expanding the values of  $\phi$  at an internal point by using expression (23). Differentiating it with respect to  $x$  and  $y$  produces

$$\frac{\partial \phi}{\partial x} = \sum_{k=1}^M \frac{\partial \mathfrak{S}_k}{\partial x} \beta_k \quad \text{and} \quad \frac{\partial \phi}{\partial y} = \sum_{k=1}^M \frac{\partial \mathfrak{S}_k}{\partial y} \beta_k \quad (24)$$

Applying Eq.(23) at all  $M$  nodes, a set of equations is produced that can be represented in matrix form by

$$\phi = \mathfrak{S} \beta \quad (25)$$

with corresponding matrix equations for Eqs.(24) and (25) given as

$$\frac{\partial \phi}{\partial x} = \frac{\partial \mathfrak{S}}{\partial x} \mathfrak{S}^{-1} \phi \quad \text{and} \quad \frac{\partial \phi}{\partial y} = \frac{\partial \mathfrak{S}}{\partial y} \mathfrak{S}^{-1} \phi \quad (26)$$

Eq.(22) then takes the form

$$(H - P) \phi = Gq \quad (27)$$

where

$$P = S \left( P_x \frac{\partial \mathfrak{S}}{\partial x} + P_y \frac{\partial \mathfrak{S}}{\partial y} \right) \mathfrak{S}^{-1} \quad (28)$$

The coefficients of the perturbation matrix  $P$  are all geometry-dependent only. Therefore, the boundary conditions can be implemented to Eq.(28) and the resulting system of algebraic equations solved by a direct or iterative scheme. It should be mentioned that, normally the approximation of  $\phi$  using constant boundary element is accurate but for the normal derivatives is less accurate and has an oscillation at the edges of the boundary which is typical for this kind of element mesh.

**7. Choice of radial basis functions**

60 In recent years, the theory of radial basis functions (RBFs) has undergone intensive research and enjoyed considerable success as a technique for interpolating multivariable data and functions. A radial basis function,  $\Psi(x - x_i) = \psi(\|x - x_j\|)$  depends upon the separation distances of a sub set of data centres,  $X \subset \mathfrak{R}^n, \{x_j \in X, j = 1, 2, \dots, N\}$ . The distance,  $\|x - x_j\|$ , are usually taken to be the Euclidean metric, although other metrics are possible (for more details see Golberg and Chen [16]). The type of RBF used  
65 in the interpolation of the unknown variables normally plays an important role in determining the accuracy

of the DRM [17]. Partridge et al. [1] have shown that a variety of functions can in principle be used as global interpolation functions  $f_k$ . The approach used by Wrobel and DeFigueiredo [4] was based on practical experience rather than formal mathematical analyses and motivated by a previous successful experience with axisymmetric diffusion problems in which a similar approach was used [18]. In the present work, decision  
70 has been made to follow [15] by starting with a simple form of the particular solution  $\psi$  and find the related expression for function  $f$  by substitution directly into Eq.(17). The resulting expressions are

$$\psi = r^3,$$

$$\eta = 3 r [(x - x_k) n_x + (y - y_k) n_y]$$

$$f = 9 D r - 3 r [(x - x_k) v_x + (y - y_k) v_y] - k r^3$$

in which  $(x_k, y_k)$  and  $(x, y)$  are the coordinates of the  $k^{th}$  boundary or internal point and a general point,  
75 respectively. It is important to notice that the set of functions  $f$  produced depend not only on the distance  $r$  but also on the diffusivity  $D$ , velocity components  $v_x$  and  $v_y$  as well as the reaction rate  $k$ , therefore, it will behave differently when diffusion or convection is the dominating process.

The most popular RBFs are labelled as:  $r^{2m-2} \log r$  (generalised thin plate spline),  $(r^2 + c^2)^{m/2}$  (generalised multiquadric) and  $e^{-\beta r}$  (Gaussian) where  $m$  is an integer number and  $r = \|x - x_j\|$ . Duchon [19]  
80 derived the thin plate splines (TPS) as an optimum solution to the interpolation problem in a certain Hilbert space via the construction of a reproducing kernel. It is interesting to observe that Duchon's thin plate splines function with  $m = 2$  corresponds to the fundamental solution commonly used in the BEM technique to solve biharmonic problems.

Another popular RBF for the DRM is the multiquadric (MQ). However, despite MQs excellent perfor-  
85 mance, it contains a free parameter,  $c$ , often referred to as the shape parameter. When  $c$  is small the resulting interpolating surface is pulled tightly to the data points, forming a cone like basis functions. As  $c$  increases, the peak of the cone gradually flatten. The multiquadric functions with values of  $m = 1$  and  $c = 0$  are often referred to as conical functions and, with  $m = 3$  and  $c = 0$ , as Duchon cubic. Even though TPS have been considered optimal in interpolating multivariate functions, they do only converge linearly, Powell [20]. On  
90 the other hand, the multiquadric (MQ) functions converge exponentially as shown by Madych and Nelson [21]. However, the tuning of the free parameter  $c$  can dramatically affect the quality of the solution obtained. Increasing the value of  $c$  will lead to a flatter RBF. This will, in general, improve the rate of convergence at the expense of increased numerical ill-conditioning of the resulting linear system [21]. Much effort has been made to search for ideal shape parameter  $c$  when utilising the multiquadric radial basis function. This  
95 is due to the lack of information on choosing the best shape parameter available in the literature, forcing the user having to make an 'ad-hoc' decision. It is important to note that the value of the multiquadric shape-parameter,  $c$ , has not been explicitly defined (see table(1)). After a process of investigation, the authors found the optimal value of the shape parameter for the current problems to be  $c = 75$ . The radial

Table 1: Radial Basis Functions

Name	Function
multiquadric MQ	$(r^2 + c^2)^{1/2}$
Thin Plate Spline TPS	$r^2 \log r$
Cubic RBF	$r^3$

basis functions presented in table(1) have been examined in this paper. Thin-plate splines (TPS) and the  
100 multiquadric are conditionally positive definite functions (for more details see [22]).

## 8. Error indicators

The accuracy of numerical solutions is usually improved by mesh refinement, as in FDM, FVM and the  
FEM. In our context there are two ways to present the solution convergence and accuracy, either by root  
mean square error or using average relative error. Our goal here is to study the convergence rates to show  
105 accuracy and the convergence of the proposed method for which results are reported.

In order to estimate the simulation error throughout the numerical experiments, the root mean square  
norm is utilised as shown below. It is based on the difference between the simulation results  $\phi_{numer}$  and the  
analytical solution  $\phi_{exact}$  as

$$RMS = \sqrt{\frac{1}{N} \sum_{i=1}^N \frac{(\phi_{i,numer} - \phi_{i,exact})^2}{\phi_{i,exact}^2}} \quad (29)$$

To obtain a more transparent measure of solution error, a well-known indicator has been used as an  
average relative error which is defined as

$$err(\phi) = \frac{1}{N} \sum_{i=1}^N \left| \frac{\phi_{i,numer} - \phi_{i,exact}}{\phi_{i,exact}} \right| \quad (30)$$

where  $i$  denotes a nodal value,  $\phi_{i,exact}$  is the analytical solution,  $\phi_{i,numer}$  is the numerical solution from the  
boundary element analysis and  $N$  is the total number of boundary and internal nodes, was computed for  
each analysis.

## 9. Numerical applications and discussions

110 The present section is concerned with the numerical application of the DRBEM for the solution of steady-  
state convection-diffusion-reaction problems with variable velocity. We shall examine several test examples  
to assess the accuracy and the performance of the proposed method.

9.1. Two-dimensional convection-diffusion-reaction problem over square region with mixed (Neumann-Dirichlet) boundary conditions and linear variable velocity

115 This example, although one-dimensional, is treated here as a two-dimensional convection-diffusion-reaction problem with a variable velocity field in the  $x$ -direction. The velocity  $v_x$  is a linear function of  $x$  expressed as

$$v_x(x) = kx + c_1$$

where

$$c_1 = \ln\left(\frac{\phi_1}{\phi_0}\right) - \frac{k}{2}$$

The problem geometry and discretisation are schematically described in fig.(1). The problem is modelled  
 120 as a square region with unit side length and mixed boundary conditions (Neumann-Dirichlet). There is no flux in the  $y$ -direction and the values  $\phi_0 = 300$  and  $\phi_1 = 10$  are specified at the faces  $x = 0$  and  $x = 1$ , respectively, with the diffusivity coefficient taking the value  $D = 1$ . The problem is discretised with 720 constant elements, 180 on each face, and 19 internal points. The exact solution of the problem is given by

$$\phi = 300 e^{\left(\frac{k}{2}\right)x^2 + c_1 x}$$

The plots of the variation of the concentration profile  $\phi$  along the  $x$ -direction are presented in figures

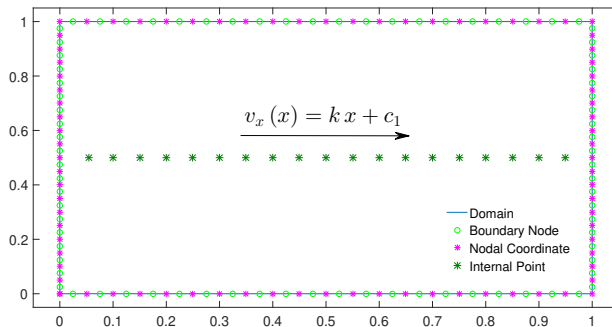


Figure 1: Domain discretisation with boundary conditions and internal nodes of square region with linear velocity problem

125 (2) to (5) for the cases  $k = 1$  to  $k = 100$ . For  $k = 1$  the velocity  $v_x$  varies from  $v_x = -2.9012$  for  $x = 1$  to  $v_x = -3.9012$  for  $x = 0$  while for  $k = 5$  the total velocity  $v_x$  varies from  $v_x = -0.9012$  for  $x = 1$  to  $v_x = -5.9012$  when  $x = 0$ . It can be noticed that the agreement with the analytical solution is very good. For the largest value of the reaction  $k = 100$ , the velocity  $v_x$  varies between  $v_x = 46.5988$  for  $x = 1$  and  $v_x = -53.4012$  when  $x = 0$ . For all these cases the average velocity is  $\bar{v}_x = -3.401$ . It is obvious that, as  
 130 the velocity increases, the concentration profile distribution becomes steeper and more difficult to reproduce with numerical models. The maximum global Péclet number for this case study is 53.4012 for  $k = 100$ . The first case study considered  $k = 1$  and an average velocity  $\bar{v}_x = -3.901$  for all nodes. The results of the

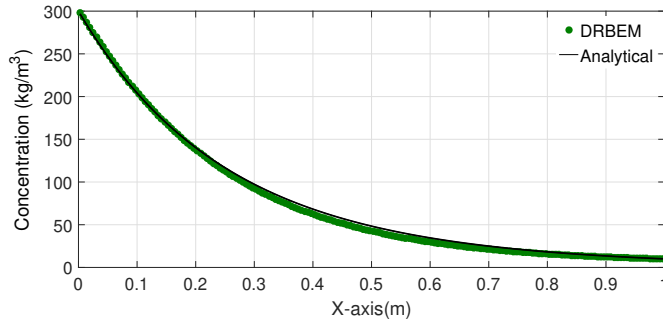


Figure 2: Variation of concentration profile  $\phi$  along face  $y = 0$  and  $y = 1$ , with  $k = 1$  using TPS-RBF: comparison between the analytical (solid line) and numerical (circle points) solutions

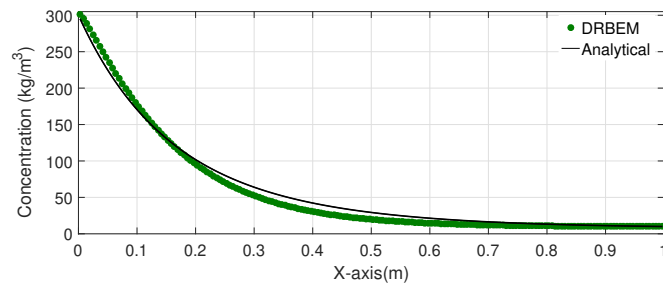


Figure 3: Variation of concentration profile  $\phi$  along faces  $y = 0$  and  $y = 1$ , with  $k = 5$  using TPS-RBF: comparison between the analytical (solid line) and numerical (circle points) solutions

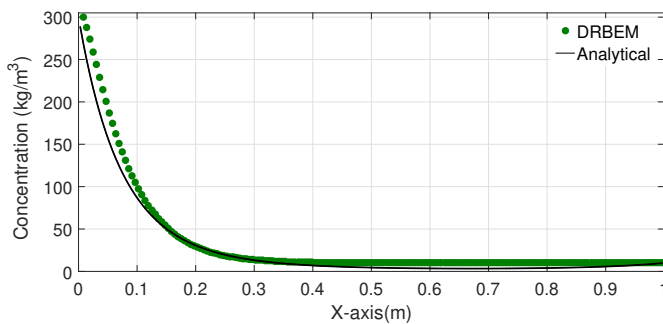


Figure 4: Variation of concentration profile  $\phi$  along faces  $y = 0$  and  $y = 1$  with  $k = 20$  using TPS-RBF: comparison between the analytical (solid line) and numerical (circle points) solutions

analyses using the three RBFs are shown in Table (2). The TPS and MQ-RBFs yield the most accurate results while the cubic-RBF is the least accurate. The relative errors for this test case using TPS are shown in fig.(6) for  $k = 5$ . Moreover, another RMS error analysis has been done for different reaction values using TPS as shown in Table (3). The RMS error increases with high  $k$ , which produces higher values of the Péclet number. The numerical evaluations of the modified Bessel functions of the second kind with zero and first orders  $K_0$  and  $K_1$ , respectively, are performed by using the Matlab built-in functions.

To assess the convergence of the boundary concentrations with mesh refinement, Table (4) presents the

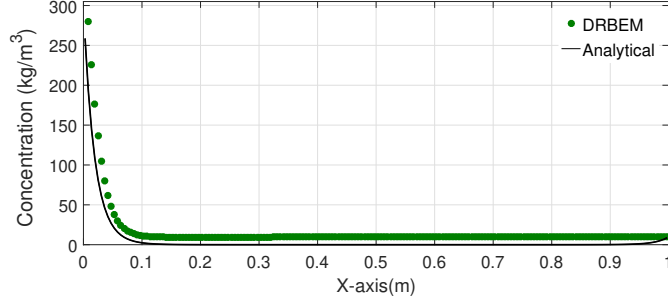


Figure 5: Variation of concentration profile  $\phi$  along faces  $y = 0$  and  $y = 1$  with  $k = 100$  using TPS-RBF: comparison between the analytical (solid line) and numerical (circle points) solutions

Table 2: Results of convection-diffusion-reaction with average velocity  $\bar{v}_x = -3.901$

x	Cubic	MQ	TPS	Analytical
0.0	300	300	300	300
0.105	215.263	201.341	201.374	200.270
0.205	153.027	135.00	134.984	137.696
0.305	108.764	90.564	90.545	95.624
0.405	77.457	61.158	61.139	67.075
0.505	55.282	41.832	41.815	47.522
0.605	39.532	29.189	29.174	34.007
0.705	28.321	20.843	20.932	24.580
0.805	20.307	15.580	15.572	17.945
0.905	14.460	12.105	12.101	13.233
1.0	10	10	10	10

Table 3: RMS error for convection-diffusion-reaction with different reaction  $k$  values

$f = r^2 \log(r)$ , Problem 1			
	$k = 1$	$k = 5$	$k = 20$
RMS error in $\phi$	0.0730	0.1611	0.7623

140 RMS results using TPS-RBF. The results indicate good convergence in the RMS norm.

### 9.2. Two-dimensional convection-diffusion-reaction problem over a unit square channel with mixed (Neumann-Dirichlet) boundary conditions and non-linear variable velocity field

In this second problem, the solution domain is taken to be the unit square  $\Omega = (0, 1) \times (0, 1)$  as described in fig.(7). The boundary is discretised with 160 constant elements, 40 on each face, and 209 internal points  
 145 adopted. A uni-directional velocity field in the  $x$ -direction depending on the coordinate  $y$  was defined by

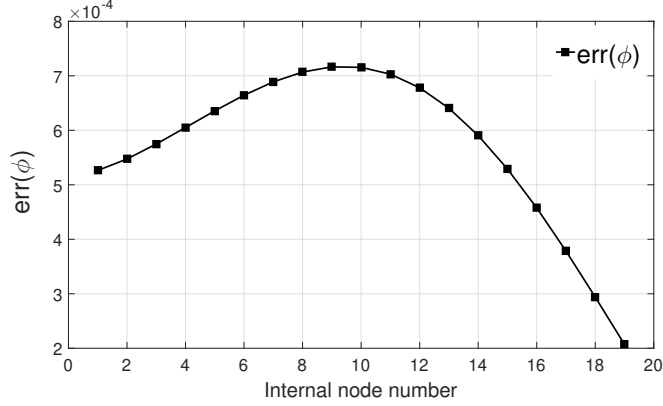


Figure 6: Relative error  $err(\phi)$  at internal nodes for 2D convection-diffusion-reaction problem

Table 4: RMS norm of DRBEM for convection-diffusion-reaction problem with different meshes

RMS error norm in $\phi$ , $f = r^2 \log(r)$ , Problem 1			
Mesh size	$k = 1$	$k = 5$	$k = 10$
20	0.1294	0.3171	0.3354
40	0.1143	0.2736	0.2814
80	0.0987	0.2314	0.2283
100	0.0943	0.2195	0.2131
200	0.0834	0.1899	0.1737
400	0.0765	0.1708	0.1470
720	0.0730	0.1611	0.1328

the expression

$$v_x(y) = A(y - B)^2$$

The velocity field is now a second-order function of the  $y$ -coordinate, with  $A$  and  $B$  are defined as constants; the values of the other coefficients are  $D = 1$  and  $k = 0$ . The constant  $B$  defines the symmetry of the velocity field with respect to the coordinate  $y$ . If  $B = 0.5$ , the velocity and the concentration profiles are both symmetric. The analytical solution to this problem is given to be

$$\phi = \bar{\phi} e^{A^{1/3}(A^{1/3}y(B - \frac{y}{2}) + x)}$$

with  $\bar{\phi} = 300$ . The mixed boundary conditions (Neumann-Dirichlet) corresponding to the problems are defined as

$$\frac{\partial \phi}{\partial n} = q = -300 A^{\frac{2}{3}} B e^{(A^{\frac{1}{3}})x}, \quad y = 0; \quad 0 \leq x \leq 1,$$

$$\phi = 300 e^{A^{\frac{1}{3}}(A^{\frac{1}{3}}y(B - \frac{y}{2}) + 1)}, \quad x = 1; \quad 0 \leq y \leq 1,$$

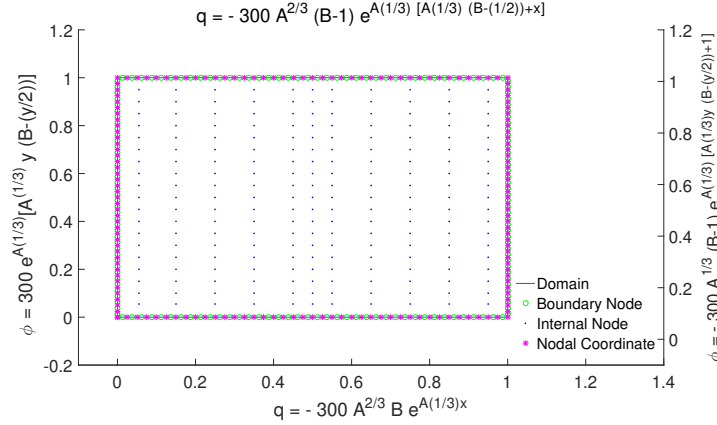


Figure 7: Geometry, discretisation, internal points and boundary conditions for two-dimensional problem with uni-directional velocity  $v_x(y)$  and side length  $1m$

150

$$\frac{\partial \phi}{\partial n} = q = 300 A^{\frac{2}{3}} (B - 1) e^{A^{\frac{1}{3}} (A^{\frac{1}{3}} (B - \frac{1}{2}) + x)}, y = 1; 0 \leq x \leq 1,$$

$$\phi = 300 e^{A^{\frac{1}{3}} (A^{\frac{1}{3}} y (B - \frac{y}{2}))}, x = 0; 0 \leq y \leq 1,$$

The average velocity  $\bar{v}_x = 0.0625$  is adopted at every node. The simulation results using the three different

Table 5: Results of convection-diffusion-reaction with average velocity  $\bar{v}_x = 0.0625$

x	Cubic	MQ	TPS	Analytical
0.15	348.505	352.465	348.438	348.550
0.25	385.185	390.817	385.120	385.207
0.35	425.715	432.487	425.651	425.720
0.45	470.507	477.825	470.416	470.493
0.55	520.009	527.268	519.860	519.975
0.65	574.718	581.322	574.491	574.662
0.75	635.188	640.580	634.902	635.100
0.85	702.301	705.738	701.765	701.894
0.95	775.985	777.993	775.891	775.712

RBFs are compared with the analytical solution in Table (5). It can be seen that the Cubic and TPS-RBFs provide results of the same level of accuracy, while the MQ-RBF shows less accurate results in this case. The RMS errors for different average velocities  $\bar{v}_x$  using TPS are shown in Table (6). Table (7) shows the RMS errors for different values of the parameter  $B$  using TPS, where it can be seen that the RMS is reduced as the value of  $B$  decreases. Table (8) shows the RMS error norm for different average velocities and mesh

Table 6: RMS error for convection-diffusion-reaction with different values of average velocity  $\bar{v}_x$

$f = r^2 \log(r)$ , Problem 2			
	$\bar{v}_x = 0.0156$	$\bar{v}_x = 0.0313$	$\bar{v}_x = 0.25$
RMS error in $\phi$	0.0016	0.0054	0.0089

Table 7: RMS error for convection-diffusion-reaction with  $A = 0.5$  and increasing values of  $B$

$f = r^2 \log(r)$ , Problem 2			
	$B = 1$	$B = 0.5$	$B = 0.25$
RMS error in $\phi$	0.0225	0.0054	0.0016

Table 8: RMS norm of DRBEM for convection-diffusion-reaction problem with different spatial meshes

RMS error norm in $\phi$ , $f = r^2 \log(r)$ , Problem 2				
Mesh size	$\bar{v}_x = 0.0156$	$\bar{v}_x = 0.0313$	$\bar{v}_x = 0.25$	$\bar{v}_x = 0.5$
20	0.0027	0.0054	0.0146	0.0244
40	0.0018	0.0043	0.0152	0.0247
80	0.0017	0.0041	0.0150	0.0241
200	0.0016	0.0041	0.0139	0.0225
400	0.00159	0.0040	0.0129	0.0211
720	0.00158	0.0040	0.0121	0.0201

sizes. It can be noticed that the errors decrease with mesh refinement. The relative error in RMS norm is just 0.001 per cent for small values of the average velocity and 0.02% for large values of  $\bar{v}_x$ .

Table 9: Results for convection-diffusion-reaction problem using MQ-RBF with different values of the shape parameter  $c$

x	c=100	c=75	c=50	c=25	c=5	Analytical
0.05	320.825	321.342	322.438	326.857	322.725	319.348
0.3	413.973	415.212	417.832	428.255	416.120	410.051
0.5	505.360	506.786	509.797	521.762	507.024	500.838
0.7	615.378	616.557	619.052	629.031	617.490	611.727
0.9	749.037	749.577	750.727	755.392	751.101	747.162

160

Table 9 shows a comparison between five different values of the shape parameter  $c$  for MQ-RBF. It is clear that the results obtained are reasonable and laying at a similar level of accuracy, with slightly better results when the parameter  $c = 75$  or  $100$ . From another point of view, as the MQ function is flattened, it will be insensitive to the radial distance  $r$ , and the elements of matrix  $\psi$  become identical. Taking a very high value of the shape parameter  $c$  generates collocation matrices which are poorly conditioned and require

165 high-precision arithmetic to solve accurately. Using a relatively high non-dimensional shape parameter of  
 75, the collocation matrices are sufficiently well conditioned to be solved using quad-precision arithmetic  
 (see [23, 24, 25] for more details on the shape parameter  $c$ ).

Case (i): The symmetric case:

The first case is considered for which the computational domain is discretised into 200 constant elements  
 170 and 209 internal points, for which fig.(8) shows the variation of the concentration profile  $\phi$  along the horizontal  
 faces  $y = 0$  and  $y = 1$  for the case  $A = 0.5$  and  $B = 0.5$ , compared to the analytical solution. Figures (9)  
 and (10) display the variation of the normal heat flux along the vertical faces  $x = 1$  and  $x = 0$ , respectively,  
 using the same value of the parameters  $A$  and  $B$ , and compared to the analytical solution.

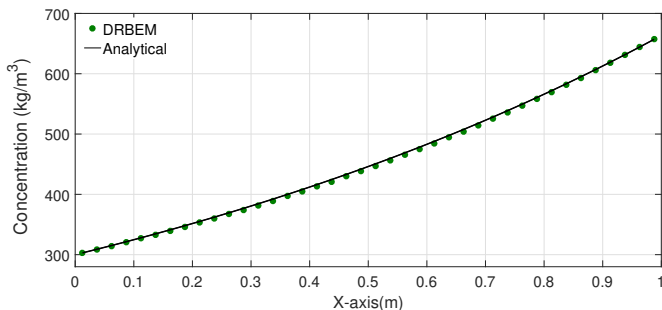


Figure 8: Variation of concentration profile  $\phi$  along faces  $y = 0$  and  $y = 1$  using TPS-RBF: comparison between the analytical (solid line) and numerical (circle points) solutions

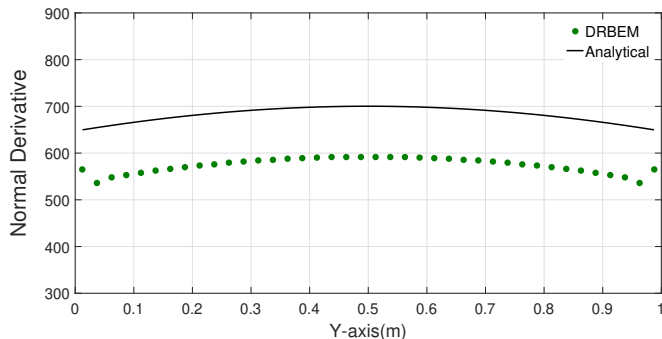


Figure 9: Variation of normal flux  $q$  along face  $x = 1$  using TPS-RBF: comparison between the analytical (solid line) and numerical (circle points) solutions

Case (ii): Non-symmetric cases:

175 The second case is implemented using the same previous discretisation but with different values for the  
 parameters  $A$  and  $B$ . Figure (11) shows the results for the concentration profile  $\phi$  along the faces  $y = 0$   
 and  $y = 1$  for the case  $A = 0.2$ ,  $B = 4$ . Figures (12) and (13) show the variation of the normal flux along  
 the vertical faces  $x = 0$  and  $x = 1$ , respectively, for this case, compared to the analytical solution. Next,  
 the value of  $B$  is considered to be  $B = 0.4$ . Figure (14) shows the variation of the concentration  $\phi$  along

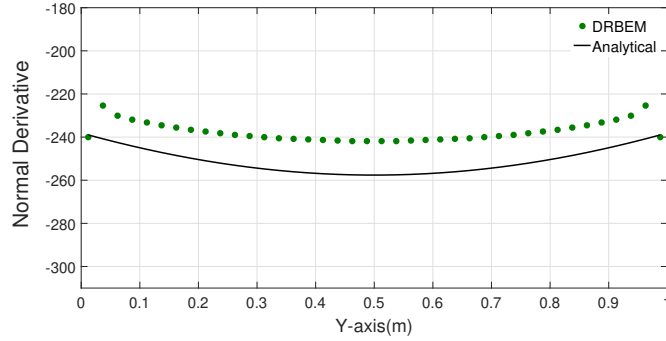


Figure 10: Variation of normal flux  $q$  along face  $x = 0$  using TPS-RBF: comparison between the analytical (solid line) and numerical (circle points) solutions

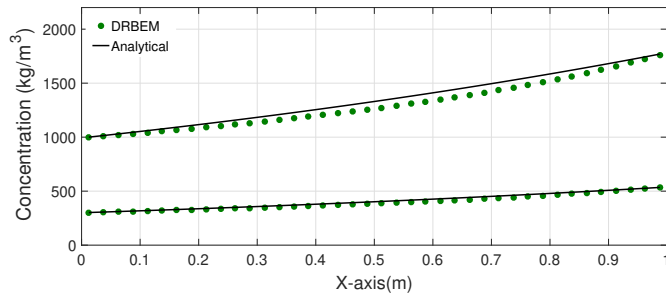


Figure 11: Variation of concentration profile  $\phi$  along faces  $y = 0$  and  $y = 1$  using TPS-RBF: comparison between the analytical (solid line) and numerical (circle points) solutions

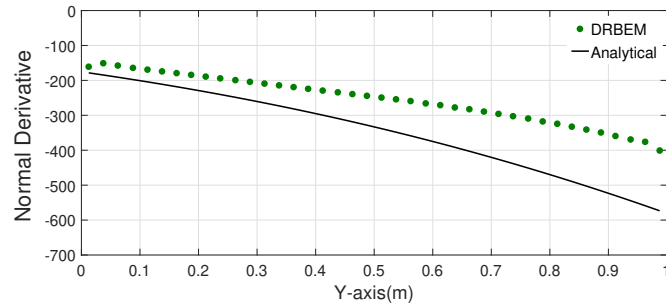


Figure 12: Variation of normal flux  $q$  along face  $x = 0$  using TPS-RBF: comparison between the analytical (solid line) and numerical (circle points) solutions

180 the horizontal faces  $y = 0$  and  $y = 1$  for the case of  $A = 0.895$ , which presents an excellent agreement with  
the exact solution. Figures (15) and (16) show the distribution of the normal heat flux along the vertical  
faces  $x = 0$  and  $x = 1$ , respectively, in comparison with the analytical solution. The oscillations near the  
boundaries are typical of the use of constant elements. Different scales are used in these figures due to the  
difference in magnitude of the fluxes. The relative error for the present study is plotted in fig.(17), for the  
185 case  $A = 0.25$  and  $B = 0.25$  with only 16 internal nodes and using TPS-RBF, which shows very accurate

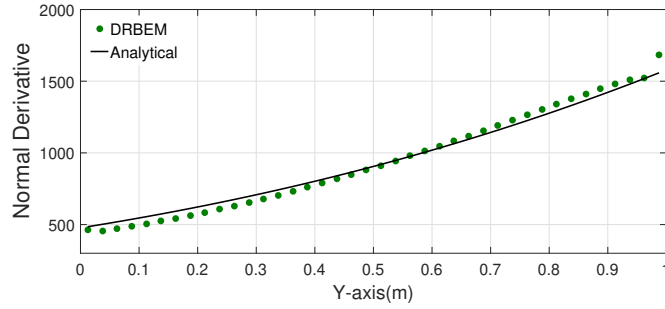


Figure 13: Variation of normal flux  $q$  along face  $x = 1$  using TPS-RBF: comparison between the analytical (solid line) and numerical (circle points) solutions

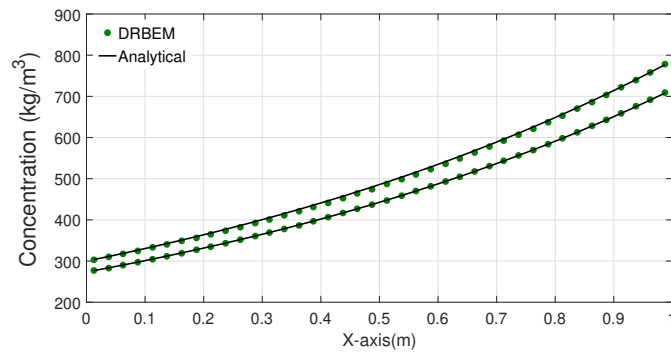


Figure 14: Variation of concentration profile  $\phi$  along faces  $y = 0$  and  $y = 1$  using TPS-RBF: comparison between the analytical (solid line) and numerical (circle points) solutions

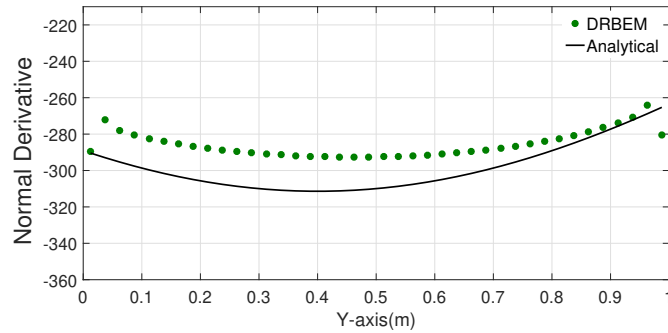


Figure 15: Variation of normal flux  $q$  along face  $x = 0$  using TPS-RBF: comparison between the analytical (solid line) and numerical (circle points) solutions

results even though using few internal nodes.

### 9.3. Two-dimensional convection-diffusion-reaction problem over a square-shaped body with mixed (Neumann-Dirichlet) boundary conditions and non-linear variable velocity field

In the last example, the cross-section is considered to be square with unit side length. This case study considers a uni-directional velocity field in the  $x$ -direction depending on the  $y$ -direction to take the following

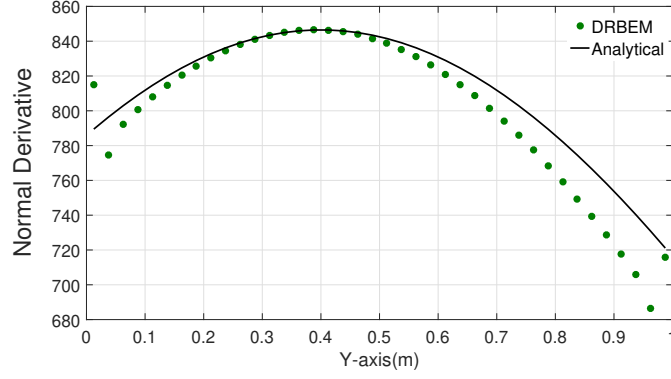


Figure 16: Variation of normal flux  $q$  along face  $x = 1$  using TPS-RBF: comparison between the analytical (solid line) and numerical (circle points) solutions

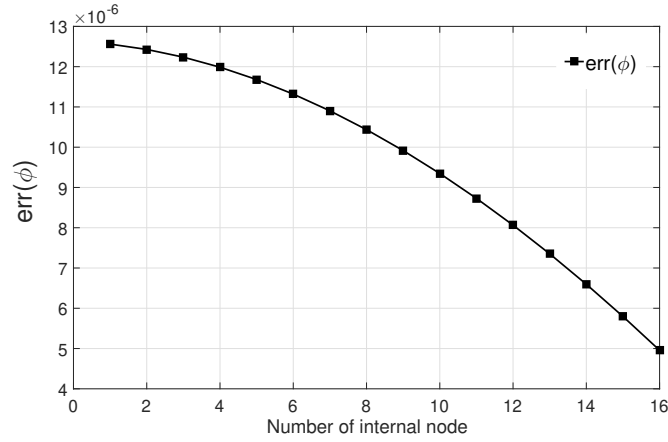


Figure 17: Relative error  $err(\phi)$  for 2D convection-diffusion-reaction problem at selected internal points

expression

$$v_x(y) = \frac{\lambda^2}{C_2} (y - B)^2 \quad (31)$$

with  $\lambda = k - C_2^2$ . The  $v_y$  component is again equal to zero and consequently the equation to be solved reduces to

$$D\nabla^2\phi - \frac{\lambda^2}{C_2} (y - B)^2 \frac{\partial\phi}{\partial x} - k\phi = 0 \quad (32)$$

subject to mixed boundary conditions (Neumann-Dirichlet) which can be defined as follows:

$$\frac{\partial\phi}{\partial n} = q = 300 \lambda B e^{(C_2 x)}, \quad y = 0; \quad 0 \leq x \leq 1,$$

$$\phi = 300 e^{(\frac{\lambda}{2} y^2 - \lambda B y + C_2)}, \quad x = 1; \quad 0 \leq y \leq 1,$$

$$\frac{\partial\phi}{\partial n} = q = 300 \lambda (1 - B) e^{\lambda((\frac{1}{2}-B)+C_2 x)}, \quad y = 1; \quad 0 \leq x \leq 1,$$

$$\phi = 300 e^{(\frac{\lambda}{2} y^2 - \lambda B y)}, \quad x = 0; \quad 0 \leq y \leq 1,$$

A particular solution to the above equation is

$$\phi = 300 \exp \left[ \frac{\lambda}{2} y^2 - \lambda B y + C_2 x \right] \quad (33)$$

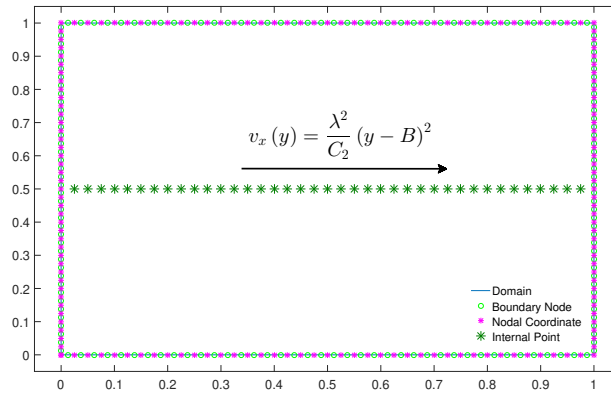


Figure 18: Domain discretisation of square-shaped body, internal points and boundary conditions with non-linear velocity problem

Table 10: Results of convection-diffusion-reaction with average velocity  $\bar{v}_x = -1.8654$

x	Cubic	MQ	TPS	Analytical
0.1	195.202	183.104	181.458	182.147
0.2	134.721	135.445	133.692	129.631
0.3	92.136	99.775	97.985	92.257
0.4	62.328	73.271	71.500	65.658
0.5	41.463	53.621	51.915	46.727
0.6	26.762	39.041	37.443	33.255
0.7	16.219	28.183	26.735	23.667
0.8	8.378	20.041	18.788	16.843
0.9	2.189	13.860	12.846	11.987

This example was studied for different average velocity values. The numerical solution when  $\bar{v}_x = -1.8654$  is tabulated in Table (10), using the three RBFs. Once again, the best results are obtained with the TPS-RBF. The value of the constant  $B$  defines the symmetry of the velocity field with respect to the coordinate  $y$ . If  $B = 0.5$  the velocity field and the concentration profiles are both symmetric. The value of the constant  $C_2$  is defined as

$$C_2 = \ln \left[ \frac{\phi(1,0)}{\phi(0,0)} \right]$$

Table 11: RMS error for convection-diffusion-reaction with increasing reaction  $k$  values

$f = r^2 \log(r)$ , Problem 3			
	$k = 5$	$k = 7.337$	$k = 10$
RMS error in $\phi$	0.2873	0.2422	0.3335

with the values  $\phi(0,0) = 300$  and  $\phi(1,0) = 10$ . Figure (18) presents the problem geometry, discretisation and internal nodes. The problem is discretised with number 160 constant elements, 40 on each face, and 39 internal points. The RMS errors for different reaction values  $k$  using TPS-RBF are shown in Table(11). The relative error at different points inside the domain with  $k = 9.724$ ,  $B = 1.4222$  and using TPS-RBF is displayed fig.(19).

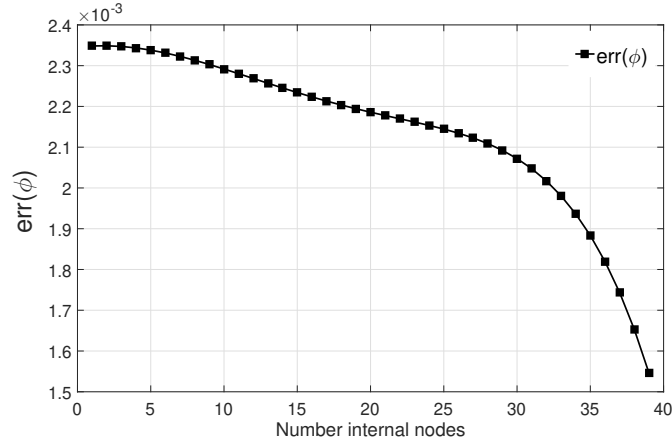


Figure 19: Relative error  $err(\phi)$  for 2D convection-diffusion-raection problem at selected internal nodes

Case(i): Non-symmetric Cases:

Figure (20) shows the concentration profile  $\phi$  at the middle of channel, where the value of  $B$  was considered as  $B = 0.222$  and the average velocity value,  $\bar{v}_x = -1.8654$ , with total velocity field  $v_x = -1.8654$  at  $y = 0$  and  $v_x = -22.9099$  at  $y = 1$ , and  $k = 0.222$ . Figure (21) represents the concentration profile when  $k = 1$

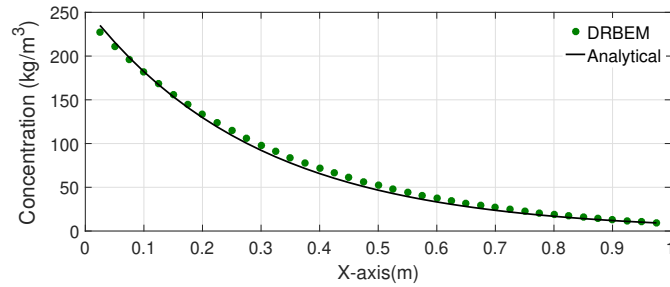


Figure 20: Variation of concentration profile  $\phi$  along the middle line of the computational domain using TPS-RBF: comparison between analytical (solid line) and numerical (circle points) solutions

along the bottom face  $y = 0$  for the case  $B = 0.125$  compared to the analytical solution. This gives velocity values of  $v_x = -0.5131$  at  $y = 0$  and  $v_x = -25.1409$  at  $y = 1$ . The maximum global Péclet number for this case is  $Pé = 25$ . Figure (22) shows simulation and exact solutions utilising the value of  $B = 1.4222$

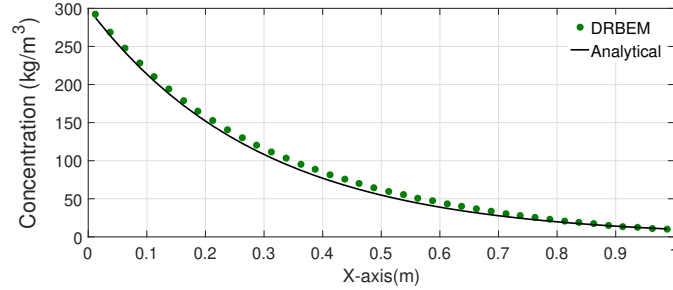


Figure 21: Variation of concentration profile  $\phi$  along the bottom horizontal face using TPS-RBF: comparison between analytical (solid line) and numerical (circle points) solutions

205

and  $k = 9.724$ . This gives velocity values of  $v_x = -2.0225$  at  $y = 0$  and  $v_x = -0.1782$  at  $y = 1$ . Next,

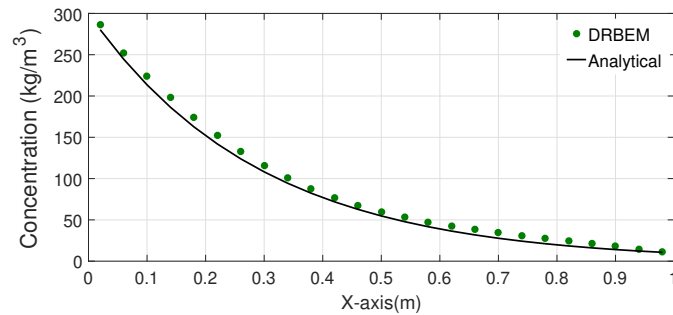


Figure 22: Variation of concentration profile  $\phi$  along the bottom horizontal face using TPS-RBF: comparison between analytical (solid line) and numerical (circle points) solutions

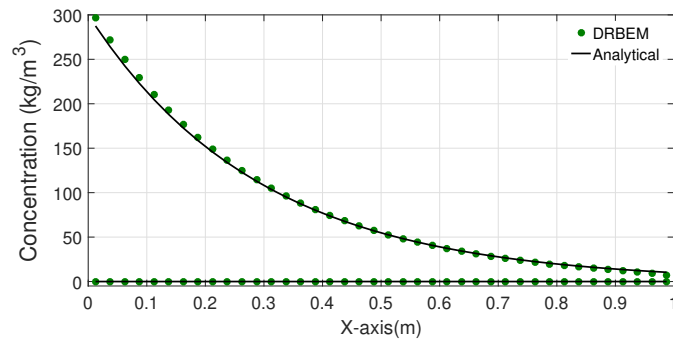


Figure 23: Variation of concentration profile  $\phi$  along the horizontal faces: comparison between analytical (solid line) and numerical (circle points) solutions

fig.(23), shows a comparison between simulation and exact solutions by utilising  $k = 50$ . The value of  $B$

was considered as  $B = 1.6$  to make the concentration  $\phi$  and the velocity profiles highly non-symmetric. This gives velocity values of  $v_x = -1.1117 \times 10^3$  at  $y = 0$  and  $v_x = -156.334$  at  $y = 1$ . Figures (24) and (25) show the variation of the normal flux  $q$  along the vertical faces  $x = 1$  and  $x = 0$ , respectively. It should

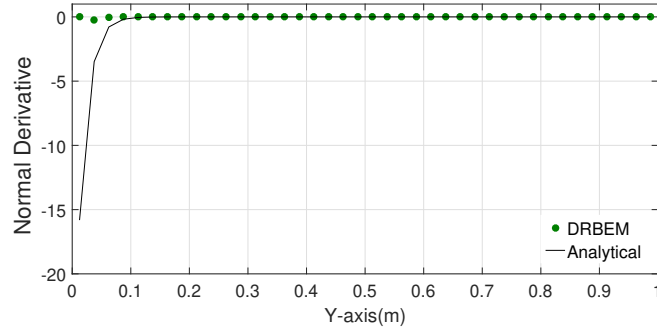


Figure 24: Variation of normal flux  $q$  along the horizontal face  $x = 1$ : comparison between analytical (solid line) and numerical (circle points) solutions

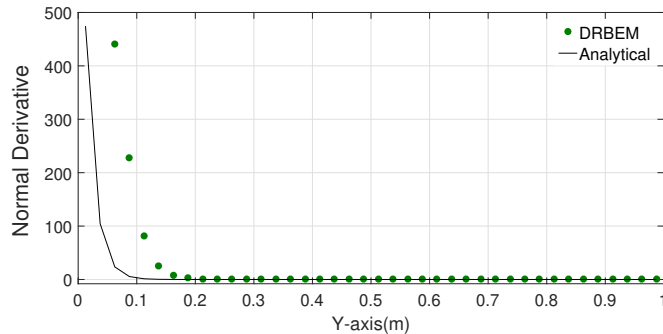


Figure 25: Variation of normal flux  $q$  along the horizontal face  $x = 0$ : comparison between analytical (solid line) and numerical (circle points) solutions

210

be stressed that the maximum global Péclet number is increased to  $Pé = 1.1117 \times 10^3$ , which is the highest value in this test case. Next, the value of  $B$  was increased to  $B = 2$ , where the velocity  $v_x = -212.178$  at  $y = 0$  and  $v_x = -53.0445$  at  $y = 1$ , whereas the reaction value was increased to  $k = 25$ . The results using TPS are in excellent agreement with the analytical solution, as shown in fig.(26). The maximum global Péclet number in this case is  $Pé = 212.178$ . Figure (27) shows the variation of the normal flux  $q$  along the vertical face  $x = 1$ . It is seen that the visible oscillations near the edges are typical of the implementation of constant boundary elements.

215

Case(ii): Symmetric case:

The last value of the parameter  $B$  was considered to be  $B = 0.5$ , where the velocity  $v_x$  and the concentration profiles become symmetric. It is found that the DRBEM gives good results with reaction value  $k = 125$  as displayed in fig.(28).

220

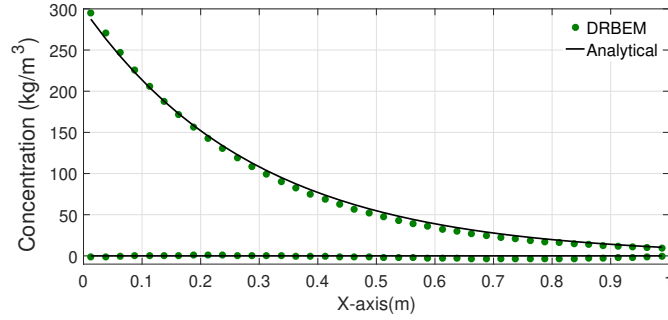


Figure 26: Variation of concentration profile  $\phi$  along the horizontal faces: comparison between analytical (solid line) and numerical (circle points) solutions

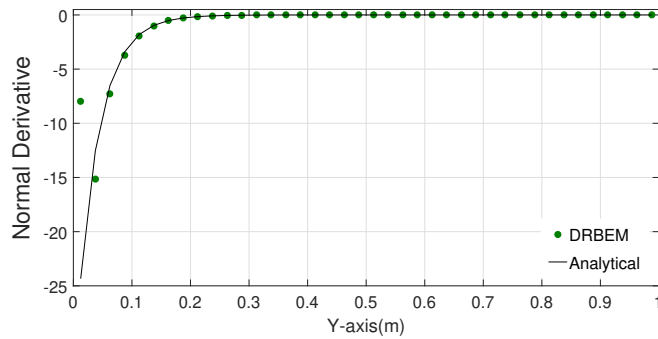


Figure 27: Variation of normal flux  $q$  along the vertical face  $x = 1$ : comparison between analytical (solid line) and numerical (circle points) solutions

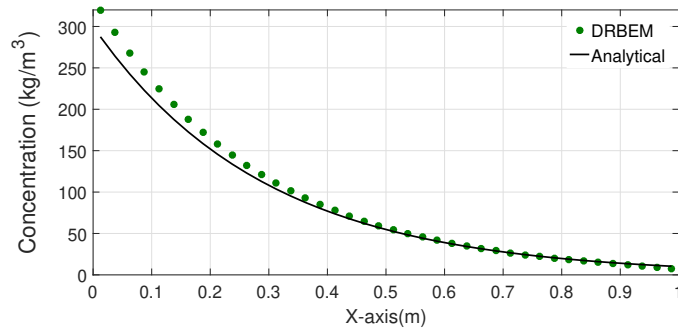


Figure 28: Variation of concentration profile  $\phi$  along the horizontal faces: comparison between analytical (solid line) and numerical (circle points) solutions

## 10. Conclusions and discussions

In this article, a BEM formulation for two-dimensional steady-state convection-diffusion-reaction problems with spatial variable velocity field is presented, employing the fundamental solution of the corresponding equation with constant coefficients and a dual reciprocity approximation of the perturbation velocity. The DRBEM is used to transform the domain integrals appearing in the BEM formulations into equivalent

boundary integrals, thus retaining the boundary-only character of the standard BEM. A proposed approach is implemented to treat the convective terms. Numerical applications are included to demonstrate the validity of the proposed technique, and its accuracy was evaluated by applying it to three tests with different velocity fields. We can note a distinct advantage of the present approach, which demonstrates very good accuracy even for high reaction values which increase the Péclet number for the cases studied. It is obvious that, as the velocity increases, the concentration distribution becomes steeper and more difficult to reproduce with numerical models. However, all BEM solutions are still accurate for a high Péclet number  $Pé = 10^3$ .

We have made an extensive investigation for the last case studied by considering many different values of the reaction coefficient  $k$ , up to  $k = 125$ . We derived and implemented three radial basis functions and tested them with different types of problems, and we have found that the thin-plate spline radial basis function is the most accurate among these RBFs for our problems. It is, however, worth stressing that the small visible oscillations of the normal fluxes at the vertical faces  $x = 0$  and  $x = 1$  in all test cases are common and distinctive for constant boundary elements. Discretisation errors of the boundary elements solutions are estimated using two different indicators to show the accuracy and effectiveness of the present method.

Previous applications of the BEM to convection-diffusion problems have shown that the BEM appears to be relatively free from oscillations and damping of the numerical solutions, which is typical of standard FDM and FEM techniques. However, since the BEM formulation requires the evaluation of singular integrals, oscillations may develop at high values of  $Pé$  if this integration is not properly carried out. Qiu et al. [6] developed a numerical technique for all BEM at high values of  $Pé$  that isolates the singular integration problem and describe the measures taken and a scheme to optimise the integration. They also show that for higher values of the Péclet number, the system matrix becomes more sparse and diagonally dominant. Thus, powerful direct or iterative solvers can be implemented for an even increased efficiency.

The numerical techniques implemented in this paper can also be applied to transient problems, as discussed in [26].

## 11. Conflict of interest statement

This work is purely academic research, and the authors declare that there are no conflicts of interest regarding the publication of this paper.

## 12. Acknowledgments

The authors would express their sincere thanks to the anonymous referees for their valuable comments and suggestions. The first author would also like to acknowledge the Ministry of Higher Education and Scientific Research of Iraq (Al-Nahrain University) for financial support and PhD scholarship.

## References

- [1] Y. Tanaka, T. Honma, I. Kaji, Mixed boundary element solution for three-dimensional convection-diffusion problem with a velocity profile, *Applied Mathematical Modelling* 11 (6) (1987) 402–410.
- [2] D. B. DeFigueiredo, L. C. Wrobel, A boundary element analysis of convective heat diffusion problems, *Advanced Computational Methods in Heat Transfer* 1 (1990) 229–38.
- [3] P. W. Partridge, C. A. Brebbia, Computer implementation of the BEM dual reciprocity method for the solution of general field equations, *International Journal for Numerical Methods in Biomedical Engineering* 6 (2) (1990) 83–92.
- [4] L. C. Wrobel, D. B. DeFigueiredo, A dual reciprocity boundary element formulation for convection-diffusion problems with variable velocity fields, *Engineering Analysis with Boundary Elements* 8 (6) (1991) 312–319.
- [5] Z. Qiu, L. C. Wrobel, H. Power, An evaluation of boundary element schemes for convection-diffusion problems, *WIT Transactions on Modelling and Simulation* 1 (1993) 25–37.
- [6] Z. Qiu, L. C. Wrobel, H. Power, Numerical solution of convection–diffusion problems at high Peclet number using boundary elements, *International Journal for Numerical Methods in Engineering* 41 (5) (1998) 899–914.
- [7] J. Ravnik, L. Škerget, A gradient free integral equation for diffusion–convection equation with variable coefficient and velocity, *Engineering Analysis with Boundary Elements* 37 (4) (2013) 683–690.
- [8] A. Shiva, H. Adibi, A numerical solution for advection-diffusion equation using dual reciprocity method, *Numerical Methods for Partial Differential Equations* 29 (3) (2013) 843–856.
- [9] S. A. Al-Bayati, L. C. Wrobel, DRBEM formulation for convection-diffusion-reaction problems with variable velocity, In: D. J. Chappell, (editor), *Eleventh UK Conference on Boundary Integral Methods (UKBIM 11)*, Nottingham Trent University Press; (2017) p. 5–14.
- [10] L. C. Wrobel, *The Boundary Element Method. Applications in Thermo-Fluids and Acoustics, Vol. 1*, John Wiley & Sons, Chichester, 2002.
- [11] P. W. Partridge, C. A. Brebbia, L. C. Wrobel, *The Dual Reciprocity Boundary Element Method*, Comp. Mech. Pub., Southampton, 1992.
- [12] M. Aliabadi, *The Boundary Element Method. Applications in Solids and Structures, Vol. 2*, John Wiley & Sons, Chichester, 2002.
- [13] J. T. Katsikadelis, *The Boundary Element Method for Engineers and Scientists: Theory and Applications*, Academic Press, 2016.

- [14] C. A. Brebbia, J. C. F. Telles, L. C. Wrobel, Boundary element techniques: theory and applications in engineering, Springer Science & Business Media, 2012.
- [15] D. B. DeFigueiredo, Boundary element analysis of convection-diffusion problems, Ph.D. thesis, Wessex Institute of Technology (1990).
- [16] M. Golberg, C. Chen, The theory of radial basis functions applied to the BEM for inhomogeneous partial differential equations, *Boundary Elements Communications* 5 (2) (1994) 57–61.
- [17] E. H. Ooi, V. Popov, Meshless solution of axisymmetric convection–diffusion equation: A comparison between two alternative RBIE implementations, *Engineering Analysis with Boundary Elements* 37 (4) (2013) 719–727.
- [18] J. C. F. Telles, A self-adaptive co-ordinate transformation for efficient numerical evaluation of general boundary element integrals, *International Journal for Numerical Methods in Engineering* 24 (5) (1987) 959–973.
- [19] J. Duchon, Splines minimizing rotation-invariant semi-norms in Sobolev spaces, *Constructive Theory of Functions of Several Variables* (1977) 85–100.
- [20] M. Powell, The uniform convergence of thin plate spline interpolation in two dimensions, *Numerische Mathematik* 68 (1) (1994) 107–128.
- [21] W. Madych, S. Nelson, Multivariate interpolation and conditionally positive definite functions. ii, *Mathematics of Computation* 54 (189) (1990) 211–230.
- [22] P. Orsini, H. Power, M. Lees, The Hermite radial basis function control volume method for multi-zones problems; a non-overlapping domain decomposition algorithm, *Computer Methods in Applied Mechanics and Engineering* 200 (5) (2011) 477–493.
- [23] A. H.-D. Cheng, Multiquadric and its shape parameter—A numerical investigation of error estimate, condition number, and round-off error by arbitrary precision computation, *Engineering Analysis with Boundary Elements* 36 (2) (2012) 220–239.
- [24] D. Stevens, H. Power, C. Meng, D. Howard, K. Cliffe, An alternative local collocation strategy for high-convergence meshless PDE solutions, using radial basis functions, *Journal of Computational Physics* 254 (2013) 52–75.
- [25] D. Stevens, H. Power, The radial basis function finite collocation approach for capturing sharp fronts in time dependent advection problems, *Journal of Computational Physics* 298 (2015) 423–445.
- [26] S. A. AL-Bayati, L. C. Wrobel, A novel dual reciprocity boundary element formulation for two-dimensional transient convection–diffusion–reaction problems with variable velocity, *Engineering Analysis with Boundary Elements* 94 (2018) 60–68.